Mapping the Lipoyl Groups of the Pyruvate Dehydrogenase Complex by Use of Gold Cluster Labels and Scanning Transmission Electron Microscopy†

Yuh-Shyong Yang,‡ Asit Datta,‡ James F. Hainfeld,§ Frederic R. Furuya,§ Joseph S. Wall,§ and Perry A. Frey*,‡

Institute for Enzyme Research, Graduate School and Department of Biochemistry, College of Agricultural and Life Sciences, University of Wisconsin—Madison, Madison, Wisconsin 53705, and Brookhaven National Laboratory, Upton, New York 11973

Received April 19, 1994; Revised Manuscript Received June 10, 1994®

ABSTRACT: This paper describes the organization of lipoyl moieties within the pyruvate dehydrogenase (PDH) complex from *Escherichia coli* as studied in the scanning transmission electron microscope (STEM). The PDH complex is a multienzyme complex consisting of E_1, pyruvate dehydrogenase, E_2, dihydrolipoyl transacetylase, and E_3, dihydrolipoyl dehydrogenase. The core of the complex is the cubic 24-subunit E_2 component, which contains the lipoyl moieties bonded to lipoyl-bearing domains. E_1 and E_3 are associated along the edges (E_1) and on the faces (E_3) of the core. The lipoyl moieties were reduced with NADH and alkylated with a *p*-maleimidobenzoyl undecagold cluster complex. The gold labels were found to be bound very nearly specifically by dihydrolipoyl transacetylase (E_2). Undecagold clusters were imaged directly by the STEM and also digitally mapped by radial mass analysis. The mass of the E_2E_3 subcomplex is about half that of the PDH complex. The PDH complex and GC-PDH are both about 420 Å in diameter, as determined by radial mass analysis, and the E_2E_3 subcomplex and GC-E_2E_3 are 320 and 350 Å, respectively. The outer boundary of the E_2E_3 subcomplex was clearly shown in STEM micrographs by the undecagold labels in GC-E_2E_3. Data obtained from radial mass analysis of GC-E_2E_3 and the unlabeled E_2E_3 subcomplex also showed that the size of the subcomplex is extended by the lipoyl-bearing domains surrounding the central E_2 core. The capabilities of lipoyl moieties to undergo translocation over long distances through structural mobility in the lipoyl-bearing domains was confirmed by the observation that many of the lipoyl groups in E_2E_3 subcomplexes relax outward into space vacated by the removal of E_1 during the preparation of the subcomplex from PDH complex. Radial mass analysis of the PDH complex and GC-PDH indicates that lipoyl groups are distributed over a large region of the PDH complex, extending from the central core to 170–180 Å from the center of the complex, with the highest density at about 75 Å from the particle centers, near the interface between E_2 and the associated components E_1 and E_3.

The PDH complex[1] catalyzes the dehydrogenation and decarboxylation of pyruvate according to eq 1. This is a complex reaction that proceeds in several steps through intermediates. In keeping with the complexity of the reaction,

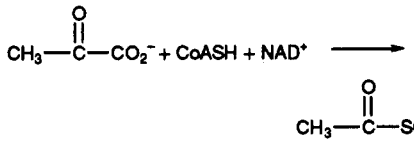

(1)

which requires decarboxylation, oxidation–reduction, and group transfer steps, this complex consists of three enzymes, pyruvate dehydrogenase (E_1), dihydrolipoyl transacetylase (E_2), and dihydrolipoyl dehydrogenase (E_3). Each component enzyme catalyzes a specific step of the overall reaction. Pyruvate dehydrogenase catalyzes the decarboxylation and dehydrogenation of pyruvate and transfer of the resulting acetyl group to dihydrolipoyl moieties on E_2. In the latter process, lipoyl moieties covalently bonded to E_2 participate as both electron and acetyl group acceptors, leading to the formation of S^8-acetyldihydrolipoyl moieties on E_2 (Yang & Frey, 1986). In the next step, E_2 catalyzes the transfer of acetyl groups from S^8-acetyldihydrolipoyl groups to CoA, forming acetyl-CoA and generating dihydrolipoyl-E_2. Dihydrolipoyl dehydrogenase (E_3·FAD) catalyzes the oxidation of E_2-bound dihydrolipoyl moieties to lipoyl-E_2 and dihydro-E_3·FAD, and finally the reduction of NAD^+ to NADH. In order to complete the overall reaction, lipoyl moieties must interact not only with E_2 itself but also with E_1 and E_3 (Reed & Cox, 1970).

The distance between the active sites of the components E_1 and E_3 has been estimated by the method of fluorescence energy transfer to be in the range of 45–60 Å (Moe et al., 1974; Shepherd & Hammes, 1977). This indicates that a

† Supported by Grant No. DK 28607 (to P.A.F.) from the National Institute of Digestive and Kidney Diseases. The STEM facility at Brookhaven National Laboratory is supported by NIH Research Resources Grant No. P41-RR01777 and by the U.S. Department of Energy.

‡ University of Wisconsin—Madison.

§ Brookhaven National Laboratory.

® Abstract published in *Advance ACS Abstracts,* July 15, 1994.

[1] Abbreviations: PDH complex, pyruvate dehydrogenase complex; E_1, pyruvate dehydrogenase; E_2, dihydrolipoyl transacetylase; E_3, dihydrolipoyl dehydrogenase; E_2E_3 subcomplex, PDH complex from which E_1 has been removed; CHES, 2-(cyclohexylamino)ethanesulfonic acid; EDTA, ethylenediaminetetraacetic acid; PMSF, phenylmethanesulfonyl fluoride; Tris, tris(hydroxymethyl)aminomethane; **1**, tricyanoheptakis-[4,4′,4″-phosphinidynetris(benzenemethanamine)]undecagold, the 0.8-nm gold cluster complex ($Au_{0.8}$); *icosa*(*N*-acetyl)-**1**, **1** with 20 amino groups acetylated and one free; *henicosa*(*N*-acetyl)-**1**, **1** with all 21 amino groups acetylated; *N*-*p*-maleimidobenzoyl-*icosa*(*N*-acetyl)-**1**, *icosa*(*N*-acetyl)-**1** with the free amino group derivatized as a *p*-maleimidobenzoyl alkylating group; maleimido-**2**, maleimde derivative of the 1.4-nm gold cluster complex ($Au_{1.4}$); NADH, reduced nicotinamide adenine dinucleotide; NAD^+, nicotinamide adenine dinucleotide; TPP, thiamin pyrophosphate; CoA, coenzyme A; acetyl-CoA, *S*-acetyl coenzyme A; GC-PDH, PDH complex labeled with the gold clusters by alkylation with *N*-*p*-maleimidobenzoyl-*icosa*(*N*-acetyl)-**1**; GC-E_2E_3, E_2E_3 subcomplex labeled with gold clusters by alkylation with *N*-*p*-maleimidobenzoyl-*icosa*(*N*-acetyl)-**1**; $GC_{1.4}$-PDH, PDH labeled with the larger gold clusters by alkylation with maleimido-**2**; NEM, *N*-ethylmaleimide; TMV, tobacco mosaic virus; STEM, scanning transmission electron microscope; SDS–PAGE, sodium dodecyl sulfate-polyacrylamide gel electrophoresis.

0006-2960/94/0433-9428$04.50/0 © 1994 American Chemical Society

simple "swinging arm" (Green & Oda, 1961; Koike et al., 1963) consisting of the lysyl and lipoyl side chains, which is about 14 Å in length, cannot fully account for electron transfer between the active sites of E_1 and E_3. Migrations of enzymatic components by a dissociation–association mechanism could in principle overcome the problem of long-distance interactions, but the exchange of E_1 components is too slow to account for any coupling reaction (Collins & Reed, 1977; Hale et al., 1979; Packman et al., 1982). Interactions among lipoyl and S^8-acetyldihydrolipoyl moieties have also been proposed (Koike et al., 1963), and the results of several experiments show that the lipoyl moieties of the complex can function as an interacting network through a relay mechanism to transfer acetyl groups and reducing equivalents from one to another over long distances (Collins & Reed, 1977; Bates et al., 1977; Angelides & Hammes, 1979; Akiyama & Hammes, 1980; CaJacob et al., 1985a).

Much evidence suggests that the lipoyl-bearing domains of E_2 are extended and flexible structures exhibiting high conformational mobility (Bleile et al., 1979; Stepp et al., 1981; Perham et al., 1981; Perham & Packman, 1989; Mattevi et al., 1992a). Thus, the enzyme-bound lipoyl moieties may be transported over long distances by the conformational mobility of the lipoyl-bearing domains of E_2. More information about the structure of the PDH complex and the properties of lipoyl-bearing domains is needed to further clarify the mechanism of interactions.

The PDH complex and its subcomplexes from *Escherichia coli* have been studied by radial mass analysis in the scanning transmission electron microscope (STEM) (Yang et al., 1985, 1986). These data provided direct evidence for the location of E_1 components along the edges and E_3 components on the faces of the cubic E_2 component. The data confirmed that E_1 and E_3 are bound at distinct sites on the E_2 core and that this placement is consistent with distances of 50–100 Å between E_1 and E_3 components. Conventional negatively stained high-resolution electron micrographs of dihydrolipoyl transacetylase showed faint fiber-like extensions from the core (Bleile et al., 1979). However, radial mass data measured on the STEM for E_2 and the E_2E_3 subcomplex indicated little mass density outside the central cores of these proteins, that is, beyond about 110 Å from the geometric centers. It is thought that extensions from the central core exhibiting very low mass density may be lipoyl-binding domains, which are responsible for transporting lipoyl groups between E_1 and E_3 components and for facilitating lipoyl–lipoyl interactions (Stepp et al., 1981). While the molecular structure of E_2 is not available, the crystal structure of the catalytic, inner domain of the homologous *Azotobacter* enzyme is available (Mattevi et al., 1992b), and the solution structure of the homologous lipoyl-binding domain from the *Bacillus stearothermophilus* enzyme has been determined by NMR (Dardel et al., (1993).

Undecagold cluster compounds carrying a single maleimide functional group are available by chemical synthesis for use in selectively modifying sulfhydryl groups of proteins (Yang et al., 1984). The undecagold clusters contain 11 gold atoms in a central core 8 Å in diameter surrounded by a shell of triphenylphosphinemethanamine ligands giving an overall diameter of 20 Å. The undecagold clusters can be imaged in the STEM (Wall et al., 1982). In the present work, the maleimido undecagold clusters are used to label the E_2-bound dihydrolipoyl complex and E_2E_3 subcomplex from *E. coli* according to Scheme 1. The distribution of undecagold-labeled lipoyl moieties within the enzyme complex is determined by use of the STEM for direct observation and radial mass

Scheme 1

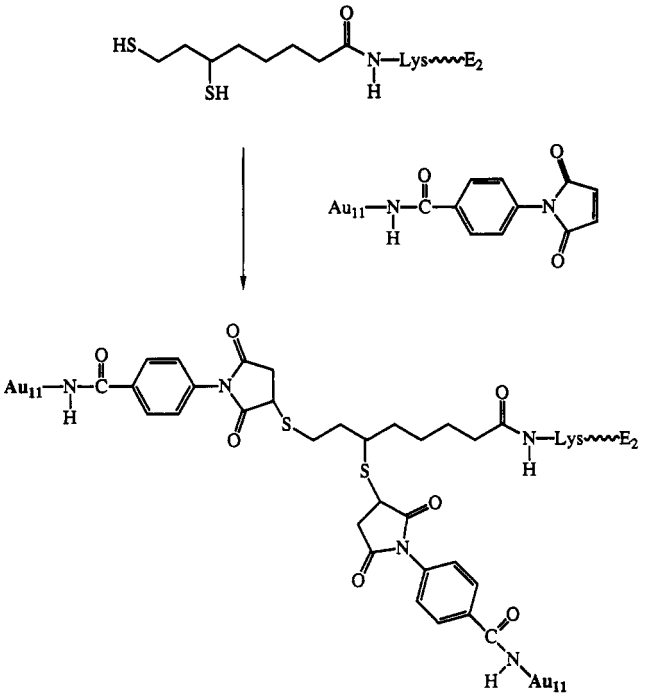

analysis. The latter allows the masses of the undecagold labels (M_r = 5680) to be mapped within the complex. The gold labels in the E_2E_3 subcomplex can be imaged and appear as bright spots in scanning transmission electron micrographs of gold cluster-labeled complexes. Many of the clusters appear outside the periphery of imaged E_2E_3 subcomplexes, consistent with the attachment of the labels to structures that are not confined to the central core structure. This distribution of gold labels is quantitatively verified by comparative radial mass analyses of the E_2E_3 subcomplex and GC-E_2E_3. In contrast, gold labels attached to lipoyl moieties in the intact PDH complex are concentrated in the central core of the complex, near the interfaces of E_1, E_2, and E_3. Similar results were obtained by use of a larger gold cluster containing a 1.4-nm gold core, which provided better visibiltiy and signal-to-noise ratio.

MATERIALS AND METHODS

Enzymes. E. coli, Crookes strain, was grown at 37 °C in 300 L media according to the procedure of Korkes (1955). The cells were stored at −70 °C after freezing in liquid nitrogen and were used within 3 days. The pyruvate dehydrogenase complex was purified from these cells by the method of Reed and Mukherjee (1969), as modified by Speckhard and Frey (1975). EDTA (1 mM) was present in all the solutions, and PMSF (2 mM) was added daily to the enzyme and buffers from a 200 mM stock solution in isopropyl alcohol. The enzyme complex was purified within 5 days and stored at −70 °C after freezing in liquid nitrogen at a concentration of about 20 mg/mL. The enzyme was assayed according to Maldonado et al. (1972) and exhibited a specific activity of 47 units/mg when the bacteria were harvested at late log phase and 62 units/mg when harvested at early log phase. SDS–PAGE of these enzyme complexes were the same regardless of the difference in specific activities. The E_2E_3 subcomplex derived from pyruvate dehydrogenase complex was eluted from a calcium phosphate gel-cellulose column by 8% ammonium sulfate after E_1 had been eluted by CHES (20 mM)–phosphate buffer at pH 9.5, a minor modification of the procedure of Reed and Willms (1966). The solution also contained EDTA

(1 mM) and PMSF (4 mM), added daily from the stock isopropyl alcohol solution. The enzyme subcomplex was stored at −70 °C after concentration by ultracentrifugation and freezing in liquid nitrogen. About 6% of the E_1 remained in this subcomplex as determined by SDS–PAGE. The enzymes were routinely checked for purity by SDS–PAGE, 10% gel with 3% stacking gel. Protein concentrations were determined by the method of Lowry (1951) or by A_{280} measurements correlated to dry weight (Speckhard, 1975).

Chemicals. Tricyanoheptakis[4,4′,4″-phosphinidynetris-(benzenemethanamine)undecagold (**1**) was synthesized as described by Bartlett et al. (1978) and was supplied by Dr. Kenneth Gruys. *N-p*-maleimidobenzoyl-*icosa*(*N*-acetyl)-**1** and *icosa*(*N*-acetyl)-**1** were prepared according to Yang et al. (1984), except that 3 mM NaCl was used to elute the *henicosa*(*N*-acetyl)-**1** from SP-Sephadex, and *icosa*(*N*-acetyl)-**1** was eluted by a linear gradient of NaCl increasing in concentration from 3 to 400 mM. Sodium cyanoborohydride was added to derivatives of **1** before desalting by passage through columns of Sephadex G-10 equilibrated and eluted with water. To prepare radioactive derivatives of **1**, [^{3}H]-acetic anhydride was used to synthesize *icosa*(*N*-[^{3}H]acetyl)-**1**. Maleimido-**2**, which is available commercially from Nanoprobes, Stony Brook, NY, was synthesized in-house. All other chemicals were purchased commercially and used without further purification.

Preparation of Undecagold Cluster-Labeled Enzyme Complexes. The lipoyl moieties of PDH complex or E_2E_3 subcomplex were reduced by NADH (1 mM) at pH 7.5 in the presence of NAD^+ (3 mM), TPP (0.3 mM), and KP_i (100 mM). The reduced enzyme complex (3–4 mg/mL) was alkylated by *N-p*-maleimidobenzoyl-*icosa*(*N*-acetyl)-**1** or by maleimido-**2** at 1 mM (12–17-fold excess over lipoyl sulfhydryl groups). The reaction mixture was dialyzed overnight against 2 mM KP_i at pH 7 in the presence of EDTA (1 mM) and PMSF (2 mM) at 4 °C to remove excess NAD^+, NADH, TPP, and undecagold labeling reagent. The desalted enzyme complex was minimally cross-linked according to the procedure of CaJacob et al. (1985b) and passed through a 0.7 cm × 18 cm gel permeation column (Bio-Gel A or Sephadex G-200) equilibrated with and eluted by 2 mM KP_i at pH 7 before being prepared for STEM analysis. In the cross-linking procedure, the complexes at 1.5 mg/mL were treated with glutaraldehyde at 0.25 wt % for 15 min at 25 °C in 2 mM potassium phosphate buffer at pH 7.0. A 2-fold molar excess (relative to glutaraldehyde) of $NaBH_4$ dissolved in 0.3 M potassium phosphate buffer at pH 8.0 was then added to destroy excess glutaraldehyde and to reduce the imine groups in the cross-links. The final concentration of phosphate buffer was 0.1 M. After 20 min at 4 °C, an 8-fold excess (relative to borohydride) of pyruvate was added to consume the unreacted borohydride, and the reaction mixture was allowed to stand for 60 min at 4 °C before being isolated from the cross-linking side products by gel filtration as described above.

Preparation of Specimens for STEM Analysis. Specimens of cross-linked proteins were prepared by adsorption onto carbon films supported by titanium grids. Freshly prepared carbon films were floated onto deionized water and picked up on holey carbon films supported on titanium grids. Samples were prepared by first placing a 2.5-μL drop of tobacco mosaic virus (TMV) solution (30 μg/mL) on the grid for 30 s. All but 0.5 μL of TMV solution was removed by touching the edge of the grid with filter paper, and a 2.5-μL drop of sample buffer was added as a wash. After a second similar wash, 2.5 μL of sample was injected into the buffer already on the grid and allowed to diffuse to the grid surface for 1 min. After this time, the grid was washed four times with deionized and distilled water or a solution of 20 mM ammonium acetate (about 10 s per wash). The wash buffer was wicked to a thickness of less than 0.1 mm, and the specimen was frozen by plunging it into liquid nitrogen slush. The use of slush minimizes boiling at the surface of the grid during the freezing process. Six such specimens were placed in an ion-pumped vacuum system, pumped to $<10^{-8}$ Torr, and warmed at 1 °C min^{-1} until the chamber pressure rose above 10^{-8} Torr. The temperature was then held essentially constant at approximately −100 °C for 4–8 h until all the ice had been sublimed and the pressure fell below 10^{-8} Torr, whereupon warming at 1 °C min^{-1} was resumed until the temperature reached 20 °C. The freeze-dried samples were transferred under vacuum into the STEM and observed at −160 °C on a cold stage. Specimen preparation as well as STEM imaging was performed at the STEM facility at Brookhaven National Laboratory.

STEM Data Analysis. STEM image data of two types were stored on magnetic tapes. One type of data was obtained with a lower electron dose (1 μm scans, with approximately 1–3 electrons/Å^2) and the other with a higher dose (0.128 μm scans, with approximately 150 electrons/Å^2). Particles that were adjacent to others or whose morphologies were drastically altered due to mass loss or damage during specimen preparation were excluded from analysis; that is, isolated and intact particles were selected for the analysis. The recorded data were displayed on a television screen connected to a digital frame buffer. Isolated particles were selected manually using a trackball driven cursor to center a circle on the particle of interest. The mass of the area enclosed by each circle was measured using TMV as the internal mass standard, after subtracting the carbon film background. The general procedure of measuring mass by STEM using a small computer system is described by Hainfeld et al. (1982). The radii of concentric measuring circles were increased from 20 Å in increments of 20 Å. Particle masses were measured as the maximum mass of a particle by using this procedure, and the data obtained on concentric measuring circles were used to construct radial mass density profiles of the particles.

In the radial mass analysis, three-dimensional spherical density profiles were constructed of the PDH complex, GC-PDH, E_2E_3 subcomplex, and GC-E_2E_3. Two types of STEM images were examined closely in these analyses, one obtained with 1 μm scans and the other with 0.128 μm scans. Our main purpose was to reconstruct three-dimensional spherical density profiles of the PDH complex and its E_2E_3 subcomplex, both undecagold labeled and unlabeled. In one approach the masses of the particles imaged at lower magnification were computed in annular rings at 20-Å intervals. From these data a spherical reconstruction can be calculated based on an algorithm described by Steven et al. (1984), yielding spherical densities at intervals of 20 Å. The method was tested with a model of a solid sphere, where the spherical density was found to be essentially constant across the diameter of the sphere, followed by a sharp decrease to zero at its edge. These methods assume the complexes are spherical (which is true to a first approximation and consistent with the resolution of this study), and all nonspherical information is averaged spherically.

With the images at higher magnification, the coordinates of the gold spots in each particle were determined after centering the particle. The positions of the gold clusters from different molecules were combined into one map, and this

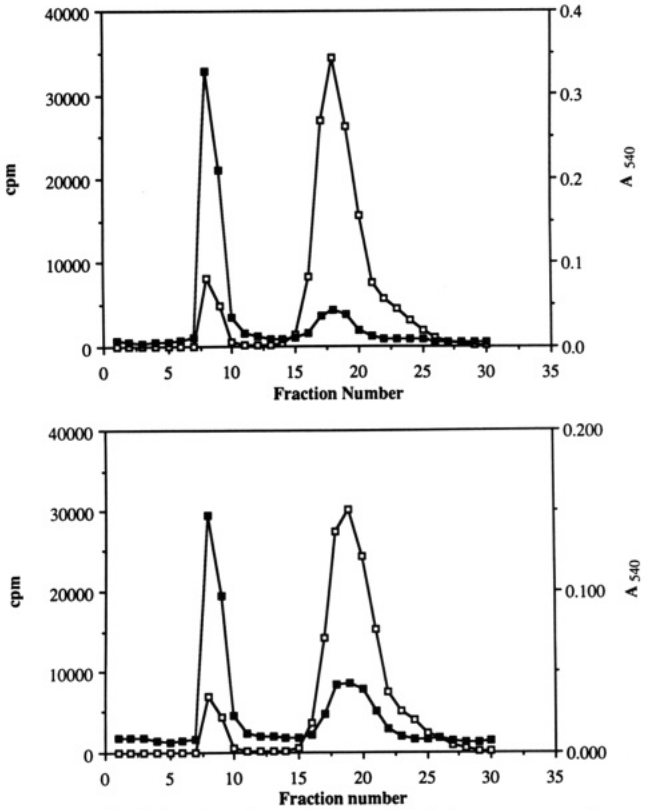

FIGURE 1: Isolation of undecagold cluster labeled enzyme complexes. The enzyme complexes were labeled with tritiated undecagold cluster (Materials and Methods) without dialysis. A 0.2-mL aliquot of the alkylation reaction mixture (0.8 mg of PDH complex or 0.6 mg of E_2E_3 subcomplex) was passed through a 0.8 × 18 cm Bio-Gel A (0.5 μm) and eluted with 0.2 mM KP_i and 1 mM EDTA at pH 7. Fractions of about 0.3 mL were collected, and 10 μL of each fraction was used to measure radioactivity and 20 μL to determine the protein concentration. (Part A, top) Elution profile of [^{3}H]GC-PDH. (Part B, bottom) Elution profile for [^{3}H]GC-E_2E_3. Symbols: (□) cpm (^{3}H-GC); (■) A_{540} (gold clusters).

composite map of spots was then divided into annular rings. From this projected distribution, the spherical density of gold as a function of radius by 3D radial reconstruction was determined as described above.

The difference in signal between the small angle elastic scattering detectors (15–40 mrad, half angle) and the large angle elastic scattering detectors (40–200 mrad) furnished additional information on the distribution of undecagold clusters that was independent of the mass measurement. This was because the large angle detectors are selectively sensitive to gold, which scatters electrons through large angles, whereas the two detectors are approximately equally sensitive to scattering by the carbon film and protein. The differences were computed and plotted versus radius to determine the distribution of undecagold clusters.

RESULTS

Preparation and Characterization of Undecagold Cluster-Labeled Enzymes. Reaction of the PDH complex or the E_2E_3 subcomplex with NADH/NAD^+ in a ratio of 1:3 reduced lipoyl-E_2 to dihydrolipoyl-E_2 while avoiding the reduction of E_3·FAD to the inactive four electron-reduced form. The dihydrolipoyl-E_2 was then alkylated by reaction with *N*-*p*-maleimidobenzoyl-*icosa*(*N*-[^{3}H]acetyl)-**1** or maleimido-**2**. The labeled proteins were separated from excess alkylating undecagold clusters by gel permeation chromatography, with the results illustrated in Figure 1. Two colored bands were

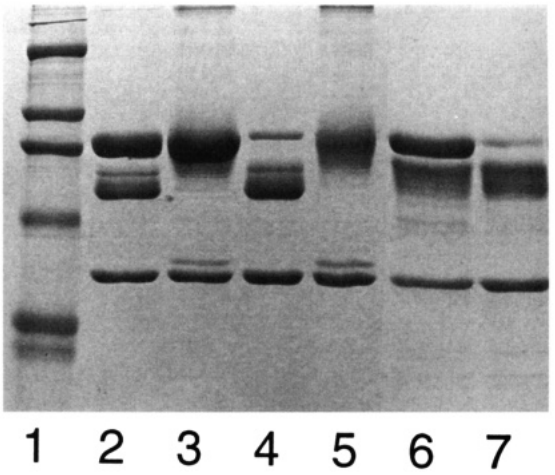

FIGURE 2: SDS–PAGE of PDH complex and E_2E_3 subcomplex. (Lanes 1–5) Samples (12 μg for [^{3}H]GC-PDH and PDH complex and 7 μg for [^{3}H]GC-E_2E_3 and E_2E_3 subcomplex) were mixed with 30 μL stock of sample solution (containing 4.6% SDS, 10% mercaptoethanol, 20% glycerol, 1.5% Tris, and 0.2% bromophenol blue in water) and heated at 37 °C for 50 min. (Lanes 6 and 7) The same amounts of proteins were mixed with 40 μL stock of sample solution plus 5 μL of mercaptoethanol and heated at 100 °C for 30 min. (Lane 1) M_r standards from top to bottom: myosin, 200K; β-galactosidase, 116.25K; phosphorylase B, 92.5K; bovine serum albumin, 66.2K; and ovalbumin, 45K. (Lane 2) PDH complex. (Lane 3) GC-PDH after denaturation at 37 °C. (Lane 4) E_2E_3 subcomplex with 6% E_1. (Lane 5) GC-E_2E_3 after denaturation at 37 °C. (Lane 6) GC-PDH after heating at 100 °C. (Lane 7) GC-E_2E_3 after heating at 100 °C.

separated by Bio-Gel A, both of which contained tritium. Only the first band eluted from the column contained protein as determined by the Lowry method. The weak A_{540} of the slow moving band in Figure 1 was due to the orange color of the undecagold cluster and not to the presence of protein. The orange color and radioactivity of the protein band showed that it was labeled with the alkylating derivative of the undecagold cluster complex.

The enzymatic components of the complex can be separated by SDS–PAGE with the results shown in Figure 2. The PDH complex gives three major bands on SDS–PAGE gels. The slowest moving and darkest band is E_1, the middle band is E_2, and the fastest moving band is E_3. When a stacking gel is used, a faint band appears between E_1 and E_2 migrating slightly slower than E_2. This appears to be related to E_2, because it is alkylated under the experimental conditions. The pattern given by the PDH complex is shown in lane 2 of Figure 2. After being labeled with the undecagold cluster, the E_2 component of the GC-PDH complex comigrates with E_1, as shown in lane 3, a fact that verifies its enhanced mass owing to the presence of the gold labels. The increase in M_r corresponds to the incorporation of approximately four undecagold clusters per subunit of E_2, in agreement with the number subject to alkylation by NEM (Danson et al., 1981). A faint band migrating slightly slower than E_3 in lane 3 of Figure 2 indicates that a small fraction of E_3 (<10%) also was alkylated. This could amount to no more than 1% of the total undecagold clusters bound to the complex. Analysis by SDS–PAGE of the E_2E_3 subcomplex (lane 4) shows the same band pattern for E_2 and E_3 as the PDH complex, but the E_1 band is almost completely absent. Analysis of GC-E_2E_3 shows that the E_2 band migrates at the same position as E_1 of the PDH complex (lane 5). After GC-PDH and GC-E_2E_3 were heated at 100 °C in air, which is known to degrade the undecagold clusters (Yang et al., 1984), the mobilities of E_2 increased,

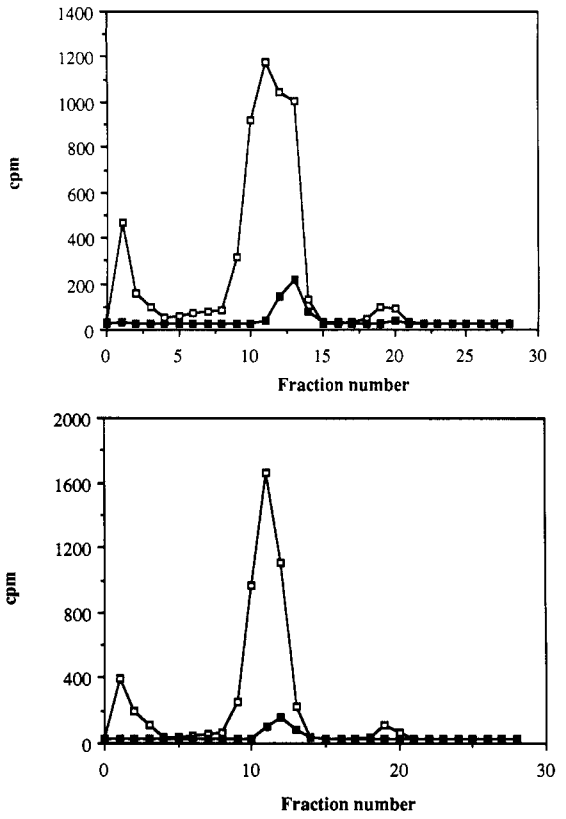

FIGURE 3: Radiochemical analysis of SDS–PAGE gel from Figure 2. Lanes from the gel in Figure 2 were excised and sliced into 2-mm sections for scintillation counting. Each gel section was mixed with 1 mL of 15% NH_4OH and heated at 37 °C overnight to solubilize the protein from gel and to decolor the stain. (Part A, top) (□) [^{3}H]-GC-PDH; (■) [^{3}H]GC-PDH heated at 100 °C for 30 min. (Part B, bottom) (□) [^{3}H]GC-E_2E_3; (■) [^{3}H]GC-E_2E_3 heated at 100 °C for 30 min.

as shown in lanes 6 and 7 of Figure 2. This represents a decrease in mass of gold-labeled E_2 as a result of the chemical decomposition of the undecagold clusters.

Lanes 3 and 5 of Figure 2 show 4–5 faint but discrete bands migrating slightly faster than the band corresponding to E_1 and labeled E_2. These presumably represent a small degree of microheterogeneity in the labeled E_2, in which some species of E_2 carry somewhat fewer labels than the maximum. The labeling conditions used in these experiments are adjusted to give near maximum but not exhaustive labeling. Complete labeling of dihydrolipoyl groups gives a high background.

The tritiated undecagold clusters (*N*-*p*-maleimidobenzoyl-*icosa*(*N*-[^{3}H]acetyl)-**1**) associated with the labeled complexes were located by radiochemical analysis of the SDS–PAGE gels with the results given in Figure 3A,B. The major part of the tritium was found to be associated with the E_1–E_2 band in the gels for GC-PDH and GC-E_2E_3. Heating these complexes at 100 °C in air, which led to slower migration of E_2 in Figure 2, also dramatically altered the radioactivity patterns. Heating greatly reduced the levels of tritium associated with E_2, and residual tritium associated with the heated complexes migrated with E_2 and not with E_1. Thus, the unheated GC-PDH in Figure 3A contained high tritium throughout the E_1–E_2 region, but the heated complex showed only a low level of tritium comigrating with E_2. Very low levels of tritium were also associated with E_3, confirming the finding in Figure 2 of low-level E_3 labeling by *N*-*p*-maleimidobenzoyl-*icosa*(*N*-[^{3}H]acetyl)-**1**. These results showed that the major site of labeling was E_2 in both the PDH complex and the E_2E_3 subcomplex.

The extent of undecagold cluster incorporated into GC-PDH and GC-E_2E_3 as estimated by their tritium contents shows that alkylation of dihydrolipoyl moieties by 1 mM *N*-*p*-maleimidobenzoyl-*icosa*(*N*-[^{3}H]acetyl)-**1** is nearly complete, 25 nmol GC/mg PDH complex and 36 nmol/mg E_2E_3 subcomplex, respectively. Partial alkylation takes place in the presence of 0.1 mM alkylating cluster, 3 and 6 nmol GC/mg protein for GC-PCH and GC-E_2E_3, respectively. Complete labeling of dihydrolipoyl moieties by NEM corresponds to the incorporation of 21 nmol of NEM per mg of the PDH complex, and 38 nmol of NEM per mg of the E_2E_3 subcomplex. This stoichiometry corresponds to the presence of two dihydrolipoyl groups per E_2 chain, which can be labeled by a maximum of four undecagold clusters per E_2 chain. Because the determination of protein concentration is affected by the undecagold clusters, these data support the labeling but are not considered to be highly accurate.

STEM Images of the Enzyme-Bound Undecagold Clusters. Shown in Figure 4 are typical examples of STEM images of the E_2E_3 subcomplex, GC-E_2E_3, PDH complex, and GC-PDH. The 0.8-nm undecagold clusters are readily observed in the particles of GC-E_2E_3. Imaging of undecagold clusters bound to the subcomplex appears to be facilitated by the fact that many of the labels are not confined to the protein core and are not overlying any protein mass. Many appear well outside the core, and some of them appear as distinct *pairs* of undecagold clusters, one bonded to each sulfur of a dihydrolipoyl moiety. The spacing between clusters in a pair averages 30 Å, which is consistent with this interpretation. Many of these clusters appear well beyond the limits of the protein images, indicating that some of the lipoyl-bearing domains project laterally from the central subunit-binding core. Some of the 0.8-nm gold clusters can be recognized as individual bright spots in images of GC-PDH. However, many of the undecagold clusters are contained within the protein boundaries of the GC-PDH, and their visibility is reduced owing to the high mass of the PDH complex (Au_{11} clusters are best seen with thin substrates). This is not a problem with the larger, 1.4-nm gold clusters, so that the individual clusters can be delineated in the images of $GC_{1.4}$-PDH shown in Figure 5.

Mapping Undecagold Complexes by Radial Mass Analysis. The projected radial mass profiles of GC-PDH, PDH complex, GC-E_2E_3, and E_2E_3 subcomplex are shown in Figure 6. The total mass of each enzyme complex or subcomplex is determined by the growth curve of radial mass. The total mass is accumulated radial mass at the point at which it ceases to increase with radius. The masses (M_r) determined are $(5.51 \pm 0.34) \times 10^6$ for GC-PDH, $(5.13 \pm 0.19) \times 10^6$ for PDH complex, $(3.43 \pm 0.6) \times 10^6$ for GC-E_2E_3, and $(2.79 \pm 0.21) \times 10^6$ for E_2E_3 subcomplex. The image radii of the PDH complex and GC-E_2E_3 are estimated to be a maximum of 275 Å. These mass differences correspond to 76 ± 53 gold clusters (MW = 5000) for GC-PDH and 128 ± 81 clusters per GC-E_2E_3.

Image sizes of these complexes, especially the E_2E_3 subcomplex, are difficult to determine by the growth curve of radial mass because of the gradual mass increase near the particle limits. Estimates of the sizes of the complexes can be obtained by analysis of the growth curves in Figure 6, and these indicate that 90% of the mass of the PDH complex is contained within a diameter of about 420 Å and that GC-PDH has the same diameter. A similar analysis for the E_2E_3 subcomplex indicates that its diameter is about 320 Å. The diameter of GC-E_2E_3 on the other hand appears to be about

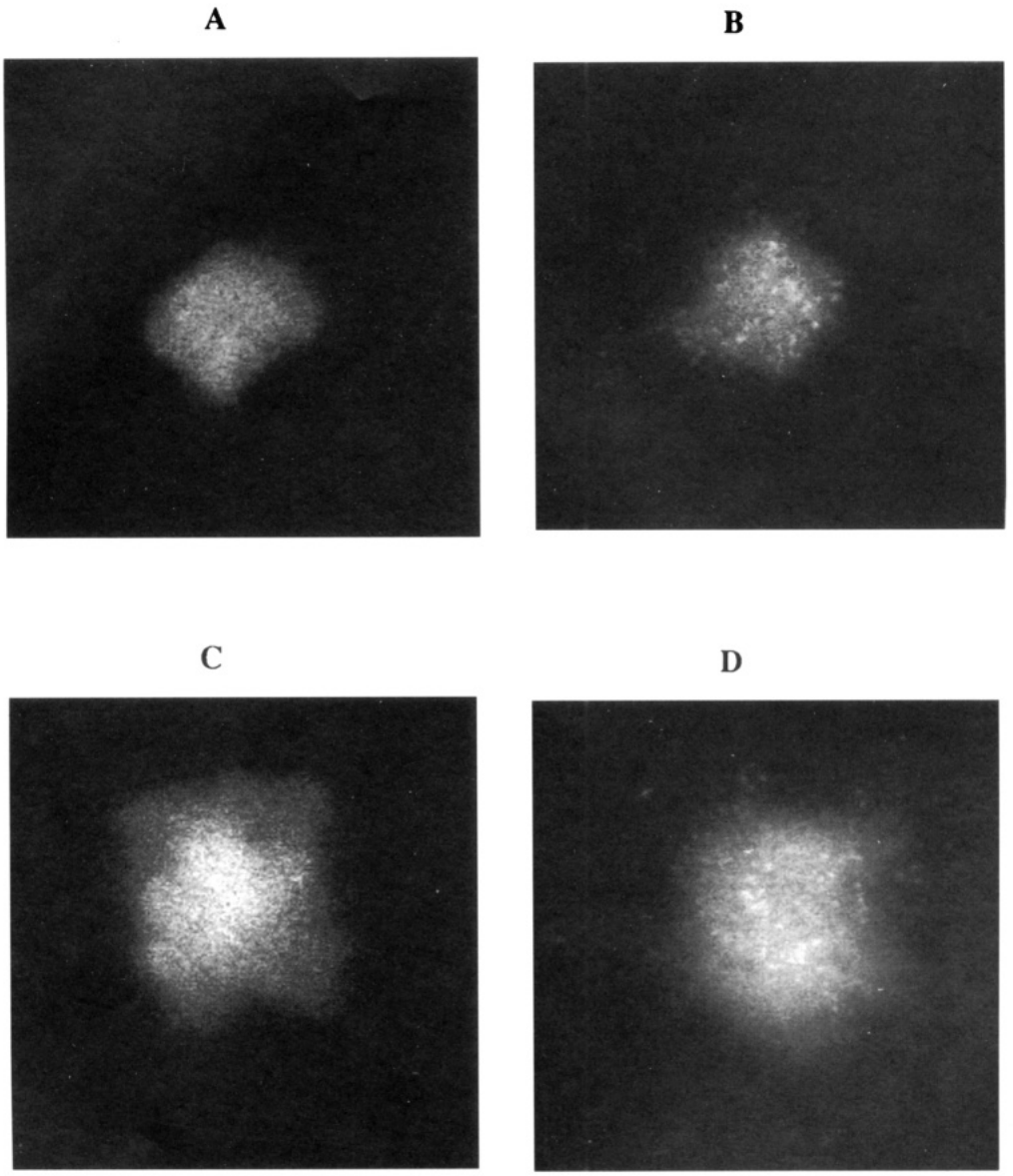

FIGURE 4: STEM images of PDH complex, GC-PDH, E_2E_3 subcomplex and GC-E_2E_3. The protein samples were prepared as described under Materials and Methods. (A) E_2E_3 subcomplex; (B) GC-E_2E_3; (C) PDH complex; (D) GC-PDH (magnification, 2.2 × 10^6).

350 Å, significantly larger than that of the E_2E_3 subcomplex itself.

A more objective analysis of the particle radii appears in Figure 7, where the three-dimensional spherical radial density profiles are plotted for the PDH complex, GC-PDH, E_2E_3 subcomplex, and GC-E_2E_3. These are plots of the mass densities for spherical shells of increasing radius centered on the particle centers versus the radii. Figure 7A shows that the mass density for the PDH complex is constant from the center of the particle to a radius of 110 Å and then gradually declines to about 5% of its center value at a radius of 210 Å, confirming the effective diameter of the particle as 420 Å. The profile for GC-PDH differs in that the mass density increases from the center to a radius of about 70 Å and then declines to near the value for the PDH complex beyond 110 Å. The difference between these two profiles indicates the distribution of undecagold complexes in GC-PDH, assuming the undecagold does not introduce a major structural perturbation in the protein complex. The simplest interpretation of Figure 7A is that the undecagold clusters are distributed throughout the central core region of the PDH complex, extending from the radius of 20 to beyond 110 Å, and they contribute maximally to the radial density at a radius of about 75 Å. The undecagold-labeled lipoyl moieties appear largely concentrated to the core region of the complex.

The spherical density profiles for the E_2E_3 subcomplex and GC-E_2E_3 in Figure 7B show that the mass densities are nearly the same within error at radii between 40 and 110 Å, but at radii of 130–170 Å the mass density for GC-E_2E_3 is significantly greater than for the E_2E_3 subcomplex. It appears that the mass density at 20 Å is slightly less for GC-E_2E_3 than for the E_2E_3 subcomplex, and the values at 40 and 60 Å may also be slightly less although the error bars overlap. The greater mass density in GC-E_2E_3 than E_2E_3 subcomplex between 130 and 170 Å arises from the absence of E_1 subunits, which contribute to the mass density in GC-PDH (Figure 7A). This is consistent with the micrograph of GC-E_2E_3 in Figure 4B, which shows a number of paired images of undecagold complexes lying outside the apparent limits of the protein core of the subcomplex.

Selective Detection of Undecagold Labels. Gold in the undecagold clusters is detected mainly by the large angle detectors of the STEM, because gold scatters electrons through large angles, whereas the large and small angle detectors are about equally sensitive to the protein and carbon film. Therefore, the undecagold labels can be selectively detected

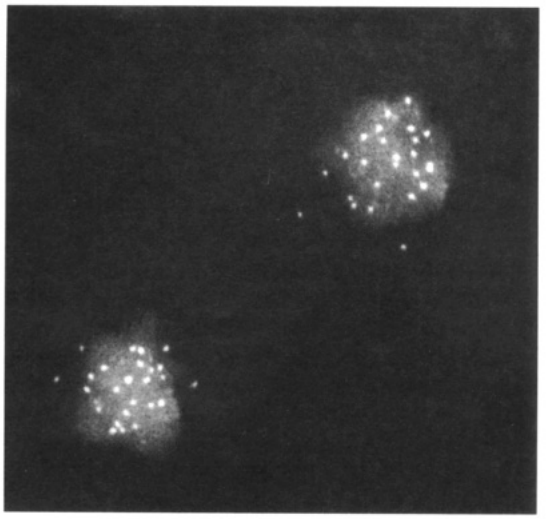

FIGURE 5: STEM image of $GC_{1.4}$-PDH. The sample was prepared as described for the GC-PDH under Materials and Methods, except for the substution of maleimido-**2** for *N*-*p*-maleimidobenzoyl-*icosa*(*N*-acetyl)-**1** as the alkylating agent (magnification, 1.1×10^6).

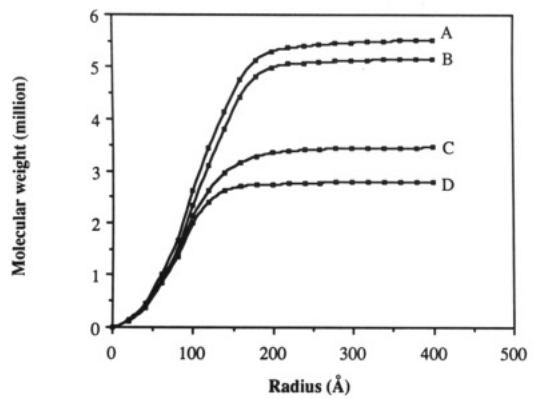

FIGURE 6: Radial mass profiles of protein complexes. The procedure for radial mass analysis is described under Materials and Methods. Each data point is the projected average accumulated radial mass, expressed as relative molecular mass (M_r), for the following number of well-defined particles of each type of complex: 37 particles of GC-PDH, 90 particles of PDH complex, 63 particles of GC-E_2E_3, and 50 particles of E_2E_3 subcomplex. Symbols: (A) GC-PDH; (B) PDH complex; (C) GC-E_2E_3; (D) E_2E_3 subcomplex.

as the difference between the signals collected by the large and small angle detectors (which will subtract the signal contribution from carbon atoms and leave a residual signal from gold). The difference can be computed from the data and plotted versus radius to obtain the radial profile for undecagold labels. This is done in Figure 8A for GC-PDH and Figure 8B for GC-E_2E_3. Also shown in Figure 8A are similar data for the PDH complex showing that the signal difference is almost constant from the center out to radii beyond 200 Å. In the case of GC-PDH the difference is a radial profile of the distribution of gold in undecagold clusters. The data confirm that the gold labels are distributed from the center of the complex to a radius of about 170 Å, with a minimum at the center and a peak between 50 and 70 Å from the particle center. The data for GC-E_2E_3 are analogous but show a more uniform distribution and extend to a radius of about 150 Å.

The maxima in Figures 7A and 8A corresponding to the location of the major part of the gold cluster labels in the PDH complex are confirmed in the radial profile for the 1.4-nm clusters bound to the PDH complex in Figure 9. The clusters are most densely concentrated at a radius of about 75 Å from the center of the PDH complex.

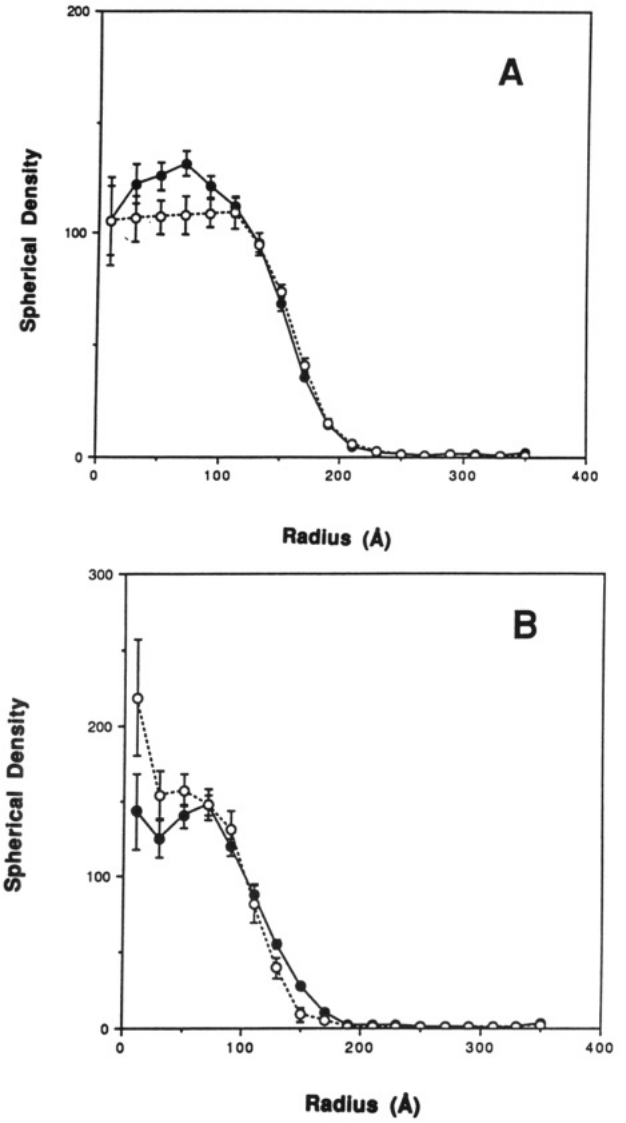

FIGURE 7: Three-dimensional radial spherical density profiles of complexes and undecagold-labeled complexes. Images of 1 μm scans (1–3 electrons/Å^2) were radially mapped, and spherical densities in in arbitrary units were determined as described under Materials and Methods. (Part A) Spherical densities are plotted versus radius for the PDH complex (○) and GC-PDH (●). (Part B) Spherical densities versus radius for the E_2E_3 subcomplex (○) and GC-E_2E_3 (●). Error bars represent the standard deviation of 16 (PDH complex) and 20 (GC-PDH) measurements on individual particles.

DISCUSSION

The STEM data reported in this research were obtained on unstained specimens that had been lyophilized on carbon films supported by grids. The STEM images were representations of the dried proteins themselves rather than of stain thicknesses surrounding the protein particles. The radiation dosages were low enough to preserve the main outlines of the image morphologies and permit mass analyses (1 – 10 e/Å^2) but were necessarily higher at higher magnifications to permit imaging of the gold clusters (10 – 100 e/Å^2).

Although the STEM data were obtained on the protein particles rather than on stain and, therefore, report directly on the structures of the particles, the interpretation of the data must take account of the method by which the specimens were prepared. The cross-linking conditions were adjusted to provide a minimum of links between the protein components of the complexes and prevent their dissociation in the course of deposition and lyophilization. The cross-links presumably

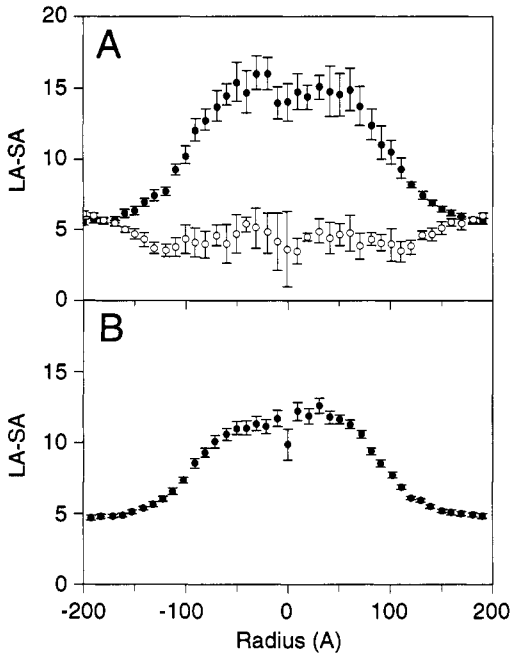

FIGURE 8: Mapping undecagold clusters in GC-PDH and GC-E_2E_3. The signal, in arbitrary units, due to gold spots alone (LA-SA) in the 0.128 μm scans of undecagold-labeled complexes was plotted against the radius. The signal due to small angle (SA) scattering was subtracted from that due to large angle (LA) scattering, taking the variation of signal with sample thickness into account. The program, which was tested against micrographs of tobacco mosaic virus, identifies the center of a protein particle and analyzes the left section of the particle separately from the right section. The bars denote the standard errors [standard deviation/$(n)^{1/2}$]. (Part A) (●) GC-PDH; (○) a control determination for the PDH complex. In the control no gold particles were present, and the essentially constant value for LA-SA reflects the fact that the large angle scattering is relatively insensitive to protein. The larger values for GC-PDH reflect the tendency of gold particles to scatter electrons through large angles, and the profile serves to map the spherical locations of gold particles. (Part B) (●) GC-E_2E_3.

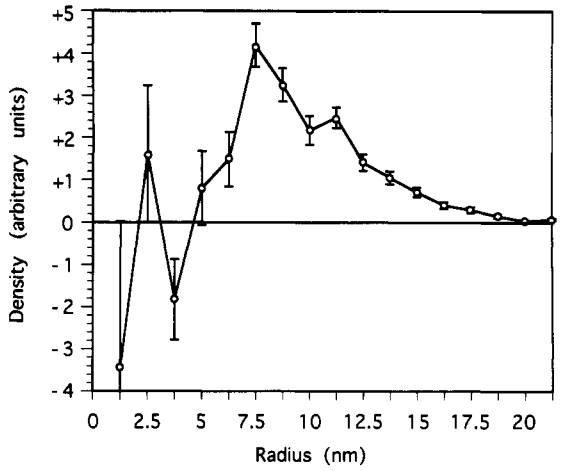

FIGURE 9: Mapping 1.4-nm gold cluster labels in PDH complex. Nearly all $Au_{1.4\ nm}$ gold cluster labels are discernible in the complex (see Figure 5). The cluster coordinates were detemined, and each cluster was assigned a mass of 1. Three-dimensional radial reconstruction was done using only the gold clusters. This resulted in a plot of the density (of the gold) at each radius (from the center of the particle) as shown in this figure. Results from 134 discrete particles were averaged to give the values and standard errors shown in this figure. A significant peak is apparent at a radius of 75 Å.

also supported the overall structures and particle morphologies during the lyophilization on carbon films. The freezing and lyophilization conditions were compatible with preservation of biochemical activity, but the effect of the carbon film on the dried particles also had to be taken into account. Hydrophobic interactions between the films and the particles probably resulted in a slight flattening and distortion of image dimensions, and image dimensions may be somewhat different than would be observed in aqueous solutions. Nevertheless, the observed images retained a high degree of order and much structural information. Therefore, we have limited the conclusions to the larger structural features rather than to high-resolution structure.

In one particular respect the STEM images must vary from the solution structures in a predictable way. The images of GC-E_2E_3 show gold clusters lying about the periphery of the central E_2E_3 core to distances up to 200 Å from the core centers. These are probably gold-labeled lipoyl-bearing domains of E_2 that have been adsorbed strongly onto the carbon film in the grid preparation process. In solution the lipoyl-bearing domains should be in motion and in all possible orientations with the labeled dihydrolipoyl groups also in many orientations. Some clusters may also become attached to the film during specimen preparation, while the complex is still subject to translational and rotational diffusion, and then be broken away from the protein. This accounts for the presence of a few gold clusters separated from particles of protein complexes at artificially high radii. Air drying, which flattens molecules by surface tension upon drying was avoided; the lyophilization used here better preserves native structure. Structure is also preserved by the limited cross-linking employed in the preparation of complexes for STEM analysis (CaJacob et al., 1985b). Nevertheless, the removal of all water may result in significant shrinkage.

The following information about the structures of the PDH complex and E_2E_3 subcomplex is provided by the STEM data obtained in this research: (1) Individual gold clusters labeling dihydrolipoyl groups in images of GC-E_2E_3 and GC-PDH can be identified and their locations mapped. (2) Images of the E_2E_3 subcomplex are the same size as those of the PDH complex when the lipoyl-bearing domains, which exhibit low mass density, are taken into account. The major protein mass is confined to a much smaller space as reported earlier (Yang et al., 1985, 1986). (3) The enzyme-bound lipoyl moieties are distributed through the images of the PDH complex and are most dense inside the interface between the central core of E_2E_3 subcomplex and the E_1 subunits bound at the edges of the cubic core. (4) Upon removal of E_1 from the PDH complex, the lipoyl-bearing domains relax away from the central core of E_2. The STEM micrographs of both GC-E_2E_3 and GC-PDH confirm that the lipoyl groups of E_2 are labeled by the undecagold clusters. The clusters represent undecagold labels attached to two –SH groups per dihydrolipoyl entity. The presence of these labels in areas beyond the periphery of the core indicates that the lipoyl groups of E_2 are bound to flexible domains, indeed on flexible "arms".

The mass measurements of M_r for the PDH complex and E_2E_3 subcomplex are in agreement with published results using STEM mass analysis, $(5.28 \pm 0.40) \times 10^6$ for the PDH complex (CaJacob et al., 1985) and $(2.76 \pm 0.22) \times 10^6$ for the E_2E_3 subcomplex (Yang et el., 1985) in the earlier work, and $(5.13 \pm 0.19) \times 10^6$ for PDH complex and $(2.79 \pm 0.21) \times 10^6$ for E_2E_3 subcomplex in this study. Two reactive lipoyl groups per E_2 chain have been reported (Danson & Perham, 1976; Collins & Reed, 1977; Speckhard et al., 1977; Danson et al., 1981; White et al., 1980), although the amino acid sequence shows the presence of three potential lipoyl-bearing domains per E_2 chain (Stephens et al., 1983). By using the subunit ratios 24:24:12 for E_1:E_2:E_3 (Moe & Hammes, 1974; Shepherd

& Hammes, 1977; Collins et al., 1977; Eley et al., 1972; CaJacob et al., 1985b), a maximum of 96 undecagold clusters can react with enzyme-bound lipoyl moieties. Assuming this number of labels, the increase in M_r for a fully alkylated enzyme complex or subcomplex will be 0.53×10^6. The observed values, $(5.51 \pm 0.34) \times 10^6$ for GC-PDH and $(3.43 \pm 0.16) \times 10^6$ for GC-E_2E_3 in this study, corresponding to 76 ± 53 and 128 ± 81 gold clusters, respectively, are in reasonable agreement, given the experimental error, with the expected mass enhancements.

The sizes of PDH complex and E_2E_3 subcomplex are known from direct measurement in electron micrographs and by radial mass analysis (Yang et al., 1985). The radial analysis in this study confirms the results for the PDH complex. For the E_2E_3 subcomplex the results are here updated by extended analysis of radial mass. Limited proteolysis and electron microscopic studies of *E. coli* dihydrolipoyl transacetylase both suggest that there is an extended structure surrounding the cube-like compact core (Bleile et al., 1979). The labeling of undecagold cluster to enzyme bound lipoyl moieties provides clear structural evidence of the extended nature of lipoyl-bearing domains.

Enzyme-bound lipoyl moieties have structural mobility as shown by EPR studies (Ambrose & Perham, 1976; Ambrose-Griffin et al., 1978), but the distance that the lipoyl groups can migrate is not clear. A long distance transfer of reaction intermediates may be required, according to the fluorescence energy-transfer measurements of the distance between active sites of E_1 and E_3 components (Moe et al., 1974; Shepherd & Hammes, 1977). Inasmuch as a 14-Å flexible arm comprising the lysyl residue and lipoyl moieties cannot span the 45–60 Å distance between E_1 and E_3 active sites, a mechanism for long distance interaction is needed. High conformational mobility of lipoyl domains has been found by ^{1}H NMR (Perham et al., 1981). On the basis of the proteolysis studies by trypsin and lipoamidase, it has been proposed that active site coupling within PDH complex depends on the movement of lipoyl domains (Stepp et al., 1981). Faint extensions from the core enzyme have been observed in negatively stained electron micrographs (Bleile et al., 1979). Extensions from the core are clearly shown by STEM micrographs of GC-E_2E_3 in Figure 4. Lipoyl moieties lying well away from the core, imaged as undecagold clusters, are accompanied by low density protein of the lipoyl-bearing domains.

The undecagold cluster-labeled lipoyl groups are quantitatively mapped by differential analysis of undecagold complexes in GC-PDH compared with PDH complex. This mapping for GC-PDH in Figure 7 indicates that the lipoyl moieties are most highly concentrated between the E_1 and E_3 components of the complex but also extend on either side of the maximum. In the absence of E_1, which in the PDH complex is associated along the edges of the cubic E_2E_3 subcomplex, some of the lipoyl moieties appear in the space normally occupied by E_1. Figures 8 and 9 indicate that the gold-labeled lipoyl moieties extend as far as about 170–180 Å from the center of the PDH complex, that is, not to the surface of the particle, which has a radius of 220 Å.

The present results enable us to map the locations of lipoyl groups within the *E. coli* PDH complex, and the results support the view that the lipoyl-bearing domains extend across a large part of the overall complex and are most dense near the interface between E_1 and E_2. They further support the proposed conformational mobility of the lipoyl domains by showing that the locations of the lipoyl groups are sensitive to the presence or absence of the E_1 components.

The lipoyl-bearing domains of the E_2 core have been biotinylated, complexed with streptavidin, and subjected to cryoelectron microscopic analysis (Wagenknecht et al., 1992). Images of streptavidin could be discerned about the periphery of 4-fold images of the E_2 core. The locations of these images indicated that the lipoyl-bearing domains may extend as much as 13 nm from the core. This is consistent with the locations of undecagold labels in GC-E_2E_3 shown in Figure 7B.

ACKNOWLEDGMENT

We thank K. Carbone, N. I. Feng, H. Chen, B. Lin, G. G. Shiue, M. N. Simon, and F. E. Kito for excellent technical assistance in STEM studies.

REFERENCES

Akiyama, S. K., & Hammes, G. G. (1980) *Biochemistry 19*, 4208–4213.

Ambrose, M. C., & Perham, R. N. (1976) *Biochem. J. 155*, 429–432.

Ambrose-Griffin, M. C., Griffin, W. G., & Perham, R. N. (1978) *Biochem. Soc. Trans. 6*, 225–226.

Angelides, K. J., & Hammes, G. G. (1979) *Biochemistry 18*, 5531–5537.

Bartlett, P. A., Bauer, B., & Singer, J. (1978) *J. Am. Chem. Soc. 100*, 5085–5089.

Bates, D. L., Danson, M. J., Hale, G. Hopper, A. E., & Perham, R.N. (1977) *Nature (London) 268*, 313–316.

Bleile, D. M., Munk, P., Oliver, R. M., & Reed, L. J. (1979) *Proc. Natl. Acad. Sci. U.S.A. 76*, 4385–4389.

CaJacob, C. A., Gavino, G. R., & Frey, P. A. (1985a) *J. Biol. Chem. 260*, 14610–14615.

CaJacob, C. A., Frey, P. A., Hainfeld, J. F., Wall, J. S., & Yang, H. (1985b) *Biochemistry 24*, 2425–2431.

Collins, J. H., & Reed, L. J. (1977) *Proc. Natl. Acad. Sci. U.S.A. 74*, 4223–4227.

Danson, M. J., & Perham, R. N. (1976) *Biochem. J. 159*, 677–682.

Danson, M. J., Hale, G., & Perham, R. N. (1981) *Biochem. J. 199*, 505–511.

Dardel, F., Davis, A. L., Laue, E. D., & Perham, R. N. (1993) *J. Mol. Biol. 229*, 1037–1048.

Eley, M. H., Namihira, G., Hamilton, L., Munk, P., & Reed, L. J. (1972) *Arch. Biochem. Biophys. 152*, 655–669.

Green, D. E., & Oda, T. (1961) *J. Biochem. (Tokyo) 49*, 742–757.

Hale, G., Bates, D. L., & Perham, R. N. (1979) *FEBS Lett. 104*, 343–346.

Hainfeld, J. F., Wall, J. S., & Desmond, E. S. (1982) *Ultramicroscopy 8*, 263–270.

Koike, M., Reed, L. J., & Carroll, W. R. (1963) *J. Biol. Chem. 238*, 30–39.

Korkes, S. (1955) *Methods Enzymol. 1*, 490–495.

Lowry, O. H., Rosebrough, N. J., Farr, A. L., & Randall, R. J. (1951) *J. Biol. Chem. 193*, 265–275.

Maldonado, M. E., Oh, K. J., & Frey, P. A. (1972) *J. Biol. Chem. 247*, 2711–2716.

Mattevi, A., de Kok, A., & Perham, R. N. (1992a) *Curr. Opin. Struct. Biol. 2*, 877–887.

Mattevi, A., Obmolova, G., Schulze, E., Kalk, K. H., Westphal, A. H., De Kok, A., & Hol, W. G. J. (1992b) *Science 255*, 1544–1550.

Moe, O. A., Lerner, D. A., & Hammes, G. G. (1974) *Biochemistry 13*, 2552–2557.

Packman, L. C., Perham, R. N., & Roberts, G. C. K. (1982) *Biochem. J. 205*, 389–396.

Perham, R. N., & Packman, L. C. (1989) *Ann. N.Y. Acad. Sci. 573*, 1–20.

Perham, R. N., Duckworth, H. W., & Roberts, G. C. K. (1981) *Nature (London) 292*, 474–477.
Reed, L. J., & Willms, C. R. (1966) *Methods Enzymol. 9*, 247–265.
Reed, L. J., & Mukherjee, R. B. (1969) *Methods Enzymol. 13*, 55–61.
Reed, L. J., & Cox, D. J. (1970) *The Enzymes (3rd Ed.) 1*, 313–240.
Shepherd, G., & Hammes, G. G. (1977) *Biochemistry 16*, 5234–5241.
Speckhard, D. C., & Frey, P. A. (1975) *Biochem. Biophys. Res. Commun. 62*, 614–620.
Speckhard, D. C., Ikeda, B. H., Wong, S. S., & Frey, P. A. (1977) *Biochem. Biophys. Res. Commun. 77*, 708–713.
Stephens, P. E., Darlison, M. G., Lewis, H. M., & Guest, J. R. (1983) *Eur. J. Biochem. 133*, 155–162.
Stepp, L. R., Bleile, D. M., McRorie, D. K., Pettit, F. H. and Reed, L. J. (1981) *Biochemistry 20*, 4555–4560.
Steven, A. C., Hainfeld, J. F., Trus, B. L., Steinert, P. M., & Wall, J. S. (1984) *Proc. Natl. Acad. Sci. U.S.A. 81*, 6363–6367.
Wagenknecht, T., Gassucci, R., Berkowitz, J., & Gorniers, C. (1992) *J. Struct. Biol. 109*, 70–77.
Wall, J. S., Hainfeld, J. F., Bartlett, P. A., & Singer, S. J. (1982) *Ultramicroscopy 8*, 397–402.
White, R. H., Bleile, D. M., & Reed, L. J. (1980) *Biochem. Biophys. Res.Commun. 94*, 78–84.
Yang, H. Reardon, J. E., & Frey, P. A. (1984) *Biochemistry 23*, 3857–3862.
Yang, H., Hainfeld, J. F., Wall, J. S., & Frey, P. A. (1985) *J. Biol. Chem. 260*, 16049–16051.
Yang, H., Frey, P. A., Hainfeld, J. F., & Wall, J. S. (1986) *Biophys. J. 49*, 56–58.
Yang, Y.-S., & Frey P. A. (1986) *Biochemistry 25*, 8173–8178.